3d-resonance-photoemission study of CeB_6 and PrB_6

S. Suga, S. Imada, H. Yamada, and Y. Saitoh
Department of Material Physics, Faculty of Engineering Science, Osaka University, Toyonaka, Osaka 560, Japan

T. Nanba
Department of Physics, Faculty of Science, Kobe University, Kobe 657, Japan

S. Kunii
Department of Physics, Faculty of Science, Tohoku University, Sendai 980, Japan
(Received 10 August 1994; revised manuscript received 15 March 1995)

A resonance-photoemission study was done for CeB_6 and PrB_6 in the region of the rare-earth $3d \rightarrow 4f$ absorption. The on-resonance spectrum has revealed reliable $4f$ photoemission structures. The hybridization of the $4f$ state and other parameters defining their electronic structures are estimated on the basis of a cluster model. It is suggested that different parts of the ligand band preferentially contribute to the hybridization with the $4f$ state in the final states of the $4f$ and $3d$ photoemission.

I. INTRODUCTION

Rare-earth hexaborides (RB_6) have so far been intensively investigated by means of transport and magnetic susceptibility measurements. RB_6 has simple cubic CsCl structure where an R atom is located at the center (Cs site) of the cube and eight octahedrons, each consisting of six boron atoms, are located at the corners. It is known that CeB_6 is a typical dense Kondo material and shows heavy fermion behavior.[1,2] Intensive band calculations were so far done on LaB_6,[3,4] since it was a practical material for an electron beam source with very low work function and also it could be a reference system with no $4f$ electron for RB_6. The band calculation by Harima *et al.*[4] well explained the fine structure of the de Haas–van Alphen experiments of LaB_6.[5] The band calculation was also performed on NdB_6.[6] The valence bands of RB_6 were systematically studied by x-ray photoemission (XPS) spectra.[7] We have recently measured the x-ray bremsstrahlung isochromat spectra in addition to the valence-band XPS and ultraviolet photoemission spectra, and briefly discussed the electronic structures of RB_6 from the viewpoint of high-energy spectroscopy.[8]

In the present paper, we discuss the electronic structures of CeB_6 and PrB_6 in more detail. In the first place, the R $3d$ and $4d$ core XPS spectra are compared with the results of multiplet calculation. Then the weak $4f$ features in CeB_6 and PrB_6 are revealed by the resonance photoemission in the R $3d \rightarrow 4f$ excitation region. The $4f$ features and the $3d$ XPS are analyzed on the basis of a cluster model calculation.

II. EXPERIMENT

The RB_6 samples were prepared by the floating zone method. The crystal structure was checked by the x-ray diffraction experiment. Magnetic, thermal, and optical measurements were done before the present study. For XPS measurement, we used an x-ray tube equipped with Al and Mg twin anodes as an excitation photon source and the photoelectron energy was analyzed by using a double-pass cylindrical-mirror analyzer. The total resolution was 0.7 eV for XPS measurement. Clean sample surfaces were obtained by scraping *in situ* with a diamond file in the ultrahigh vacuum chamber with the base pressure of $\sim 2 \times 10^{-10}$ Torr. During the XPS measurement, the cleanliness of the surfaces was checked by the absence of O $1s$ and C $1s$ photoemission signals. The surfaces were kept clean during the measurement by occasionally repeating filing.

The resonant photoemission study in the R $3d$ core excitation region was done with the use of the undulator radiation at the BL-2B beam line of the Photon Factory in KEK. The energy resolution of the photon was set to 0.6 eV. The total energy resolution was 0.8 eV for CeB_6 and 1.2 eV for PrB_6.

III. EXPERIMENTAL RESULTS

We measured the R $3d$ and $4d$ core XPS spectra and compared them with convoluted results of atomic multiplet calculation. First we measured the $3d$ spectra of LaB_6 and CeB_6. The calculation was done in the same way as by Thole *et al.*[9] for Ce^{3+} ($3d^9 4f^1$) with the parameters shown in Table I. The tails of both $3d_{3/2}$ and $3d_{5/2}$ peaks in the experiment on the smaller binding-energy (E_B) side are attributed to the well-screened states,[10,11] i.e., $3d^9 4f^1$ final state in LaB_6, and $3d^9 4f^2$ state in CeB_6, which are not treated in the present calculation. The intensities of the well-screened structures in the spectra of LaB_6 and CeB_6 are appreciably smaller than those observed in RPd_3 or R_2O_3.[10,11]

The Pr $3d$ and $4d$ core XPS spectra in PrB_6 are displayed in Figs. 1(a) and 1(b) by dots along with the multiplet calculation of the $d^9 f^2$ state. Both $3d_{3/2}$ and $3d_{5/2}$ peaks have tails on the smaller E_B side that are

characterized by the well-screened state as in the case of LaB_6 and CeB_6. In addition to these tails, it is noticed that the $3d_{3/2}$ XPS peak has a shoulder on the larger E_B side, whereas no structure is observed in the larger E_B region of the $3d_{5/2}$ XPS peak. According to the calculation, we attribute this shoulder to multiplet structures.

It is known that the intensity of the well-screened peak and the line shape of the Pr 4*d* photoemission spectrum depend on the strength of the Pr 4*f* hybridization.[11] The comparison in Fig. 1(b) shows, however, that the experimental Pr 4*d* spectrum can be reasonably explained by the multiplet calculation.

LaB_6, CeB_6, and PrB_6 nominally have 0, 1, and 2 4*f* electrons in the ground state. According to the band calculation for LaB_6,[12] a B 2*s*,2*p* state dominated by the B 2*s* state with a little hybridization with the *R* 5*d* state is located at about $E_B=10$ eV and a B 2*p*,2*s* state appreciably hybridized with the *R* 5*d* state is located at about $E_B=5$ eV. Although the B 2*p*,2*s* state hybridized with the *R* 5*d* state around $E_B=5$ eV is clearly observed in the ultraviolet photoemission spectrum at $h\nu=40$ eV in LaB_6, its energy position is not so clear in the XPS spectra of CeB_6 and PrB_6 because of the overlap with the *R* 4*f* structure. But still we see that LaB_6 has slight structures at about $E_B=10$ and 5 eV. The hump located at $E_B=10$ eV is also noticed in CeB_6 and PrB_6.

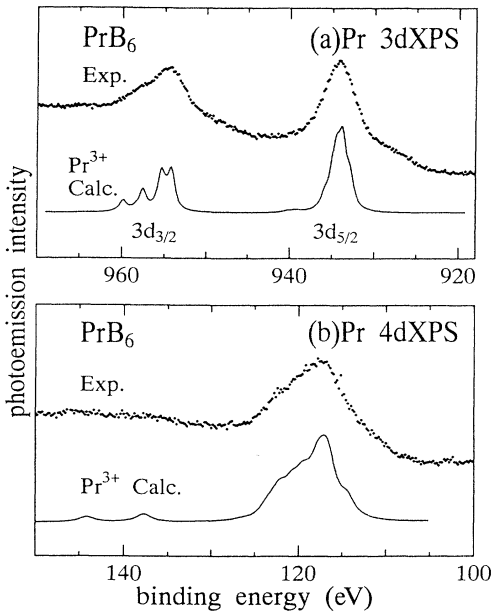

FIG. 1. XPS spectra of PrB_6 (dots) and the multiplet calculations for the d^9f^2 state (solid lines). (a) Pr 3*d* and (b) Pr 4*d* spectra.

TABLE I. The values of electrostatic interaction parameters *F*'s and *G*'s and spin-orbit interaction parameters ζ's which are used in the multiplet calculation. These values are obtained by multiplying the results of a Hartree-Slater atomic calculation by the factor *c*'s in the last column.

	Ce^{3+}	Pr^{3+}	*c*
$4f^n$			
F^2_{ff}		10.1	0.75
F^4_{ff}		6.4	0.75
F^6_{ff}		4.6	0.75
ζ_f	0.10	0.11	0.75
$3d^94f^n$			
F^2_{ff}		11.4	0.75
F^4_{ff}		7.2	0.75
F^6_{ff}		5.2	0.75
F^2_{df}	6.6	6.9	0.7
F^4_{df}	3.1	3.3	0.7
G^1_{df}	4.8	5.0	0.7
G^3_{df}	2.8	3.0	0.7
G^5_{df}	1.9	2.0	0.7
ζ_d	7.6	8.2	0.95
ζ_f	0.13	0.14	0.75
$4d^94f^n$			
F^2_{ff}		11.0	0.75
F^4_{ff}		6.9	0.75
F^6_{ff}		5.0	0.75
F^2_{df}		11.0	0.7
F^4_{df}		7.1	0.7
G^1_{df}		13.0	0.7
G^3_{df}		8.2	0.7
G^5_{df}		5.8	0.7
ζ_d		1.5	0.95
ζ_f		0.13	0.75

We next describe the resonance photoemission study of the valence-band region for the *R* $3d\rightarrow 4f$ excitation. The total photoelectron yield spectra in the *R* $3d\rightarrow 4f$ absorption region of CeB_6 and PrB_6 are given in Figs. 2(a) and 2(b). Each spectrum consists of two well-separated peaks, corresponding to the $3d_{5/2}$ (M_5) and $3d_{3/2}$ (M_4) core levels. These spectra resemble those of γ-Ce and PrF_3, respectively, reflecting the R^{3+} character. We then measured the valence-band photoemission spectra using the photons with energies marked in Fig. 2. Figure 3 summarizes the photoemission spectra of CeB_6 taken in the region of the Ce $3d\rightarrow 4f$ absorption. Spectra *C* and *D* excited around the absorption maximum consist of two peaks. These peaks correspond to the bonding and antibonding combinations of the f^{n-1} final state and $f^n\underline{L}$ final state in which the photoproduced *f* hole is screened by the B 2*p* electron through the 4*f* ligand hybridization. Here, *n* stands for the number of *f* electrons in the initial state and $\underline{L}$ denotes the B *p*-band hole. If we assume that the $d^9f^{n+1}\rightarrow d^{10}f^{n-1}+e$ Auger process takes place immediately after the $3d\rightarrow 4f$ photoabsorption, an interference will take place with the $d^{10}f^n\rightarrow d^{10}f^{n-1}+e$ photoemission. In general, the symmetry of the final state of the Auger process as well as the intensity ratios of the multiplet structures depend upon the excitation photon energy. In the case of CeB_6, however, the $d^{10}f^0$ final state for $n=1$ has no degeneracy and it has no ambiguity except for a coefficient. Hence, the intensity ratio of the two peaks depends only upon the f^0 weights in the final states. The peak positions should also be independent of the incident photon energy. In our experiment, however, the positions of the peaks and the intensity ratio depend slightly on the photon energy as seen in Fig. 3 (*C* through

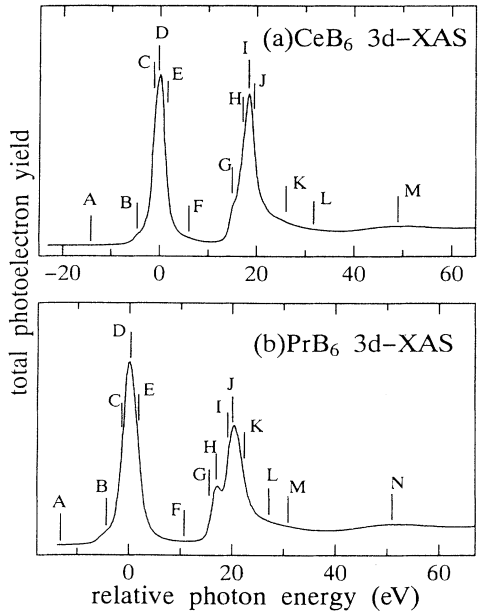

FIG. 2. R $3d \rightarrow 4f$ XAS spectrum of (a) CeB_6 and (b) PrB_6.

F and G through K). But the change of the E_B of the photoemission peak is much smaller than the difference of $h\nu$. Hence, we think that weak Auger structures are superimposed on the resonant photoemission spectrum, which has a common shape independent of the photon energy. Spectrum C in Fig. 3 excited in the smaller $h\nu$ region of the absorption peak can be considered to be least influenced by the Auger electron signal and dominated by the bonding and the antibonding combinations. Besides, we also note that some of the $h\nu$ dependence of the spectrum may take place if the f^2 component is present in the initial state, resulting in a $h\nu$ dependence of the final state.

For PrB_6, the spectra around the resonance maximum do not have clear two-peak structures, although they can be deconvoluted into two components as in Fig. 4. One might suspect whether the energy resolution being worse than that for CeB_6 (see Sec. II) made the original two-peak structure broadened. We have checked this possibility by measuring the spectrum with higher resolution and found that this is not the case.

IV. CLUSTER MODEL ANALYSIS

Next we quantitatively analyze the resonant photoemission spectrum of CeB_6 in terms of the cluster model.[13] In order to treat the $h\nu$ dependence of the resonant photoemission spectrum due to the presence of the f^2 components in the initial state, a multiplet calculation in

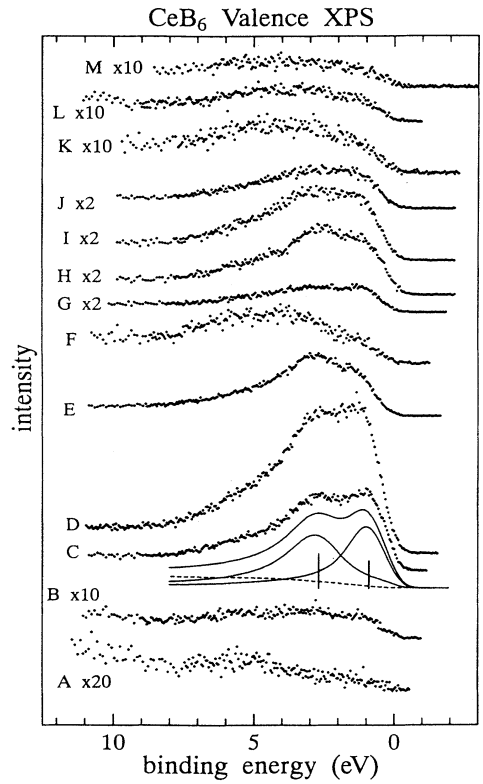

FIG. 3. Valence-band resonant photoemission spectra of CeB_6 in the Ce $3d \rightarrow 4f$ absorption region. The solid curves show the deconvolution into the antibonding and bonding components (see text for details).

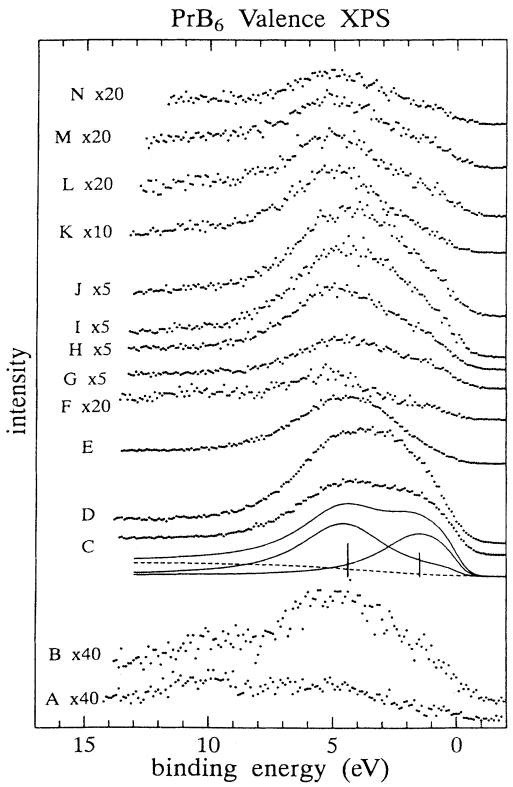

FIG. 4. Valence-band resonant photoemission spectra of PrB_6 in the Pr $3d \rightarrow 4f$ absorption region.

the cluster model will be required. But such a calculation is beyond the scope of this paper. Hence we neglect the $h\nu$ dependence and analyze spectrum C of Fig. 3 as a normal photoemission. Filled p bands derived from the ligand B and a localized f orbital of the Ce^{3+} ion are considered for a $Ce(B_6)_8$ cluster. The ligand band is represented with a single level. It is considered that this level is not situated at the mean energy of the p band but set at the energy where the p states are most strongly hybridized with the f level. The spin-orbit splitting of the f state is also neglected in the present calculation. Let us use E_f, E_L, and V to denote the energies of the unhybridized f and ligand levels and the effective transfer integral between an f state and ligand states. Due to the hybridization, the ground state consists of the $4f^1$ and $4f^2\underline{L}$ states. Then the $4f$ photoemission final states are composed of the $4f^0$ and $4f^1\underline{L}$ states. Taking the $4f$ degeneracy into account, the effective hybridization in the ground state between the $4f^1$ and $4f^2\underline{L}$ states is $v_0=\sqrt{13}V$ and that between the $4f^0$ and $4f^1\underline{L}$ final states is $v=\sqrt{14}V$, where V is assumed to be the same in the initial state and in the $4f$ photoemission final state. We first consider the matrix

$$\begin{array}{c} \\ 4f^1 \\ 4f^2\underline{L} \end{array}\begin{bmatrix} E_f & v_0 \\ v_0 & 2E_f-E_L+U_{ff} \end{bmatrix} \tag{1}$$

for the initial state. The matrix for the $4f$ photoemission final state is represented by

$$\begin{array}{c} \\ 4f^0 \\ 4f^1\underline{L} \end{array}\begin{bmatrix} 0 & v \\ v & E_f-E_L \end{bmatrix} . \tag{2}$$

The eigenenergies and eigenstates are obtained by the diagonalization of these matrices. The initial state corresponds to the lower-energy state obtained from (1) which is represented by Ψ_i,

$$\Psi_i=c_1^i|4f^1\rangle+c_2^i|4f^2\underline{L}\rangle . \tag{3}$$

The two final states are represented by

$$\Psi_{f\pm}=c_{0\pm}^f|4f^0\rangle+c_{1\pm}^f|4f^1\underline{L}\rangle . \tag{4}$$

The subscripts $-$ and $+$ correspond to the smaller and larger binding-energy peaks. The intensity of the two $4f$ photoemission peaks is then given by

$$I_{f\pm}=|c_1^{i*}c_{0\pm}^f+c_2^{i*}c_{1\pm}^f|^2 . \tag{5}$$

The binding energies corresponding to the two hybridized final states are given by

$$\begin{aligned} E_\pm=\{&E_f-E_L\pm[(E_f-E_L)^2+4v^2]^{1/2}\}/2 \\ &-\{(3E_f-E_L+U_{ff})-[(3E_f-E_L+U_{ff})^2 \\ &\qquad -4E_f(2E_f-E_L+U_{ff}) \\ &\qquad +4v_0^2]^{1/2}\}/2 . \end{aligned} \tag{6}$$

From spectrum C in Fig. 3, we have obtained the following results:

$$E_+=2.7\text{ eV},\quad E_-=0.9\text{ eV},\quad I_{f-}/I_{f+}=0.8 ,$$

where E_+, E_-, I_{f-}, and I_{f+} were evaluated by deconvoluting the spectrum into two components (see Fig. 3, spectrum C). We have obtained the best fit line spectrum which reproduces the experimental spectrum in Fig. 3, spectrum C by assuming the following line-shape function. First, we assumed a Doniach-Sunjic line shape for the two-line spectra in the following representation:

$$f(E_B)=\Gamma(1-\alpha)\cos[\pi\alpha/2+(1-\alpha)\arctan(E_B/\gamma)]/(E_B^2+\gamma^2)^{(1-\alpha)/2} ,$$

where Γ, α, and γ stand for the gamma function, asymmetry parameter, and the half width at half maximum. Second, the spectrum is multiplied by the Fermi step function at room temperature. Finally we have obtained the spectrum convoluted by the Gaussian function. In addition, we have assumed an integral type background.

The three values E_+, E_-, andI_{f-}/I_{f+} are insufficient to give a unique set of values for the four parameters V, E_f, E_L, and U_{ff}. But if we choose one of the parameters as an independent variable, the remaining three parameters are obtained as functions of it. Choosing V as an independent variable, we obtain U_{ff}, E_f, and E_L as functions of V as show in Fig. 5(a). If we assume $U_{ff}=6.4$ eV after Fuggle *et al.*,[14] we get from this figure the following values (in eV): $V=0.22(3)$, $E_f=-2.0$, and $E_L=-1.4$.

We now analyze the $3d$ XPS spectrum of CeB_6 using the same method and try to find a consistent explanation of the $3d$ and the $4f$ photoemission. We assume that the final states are the bonding and antibonding combinations of the $3d^94f^1$ and $3d^94f^2\underline{L}$ states. These states are the eigenstates of the matrix

$$\begin{array}{c} \\ 3d^94f^1 \\ 3d^94f^2\underline{L} \end{array}\begin{bmatrix} -E_d+E_f-U_{fc} & v' \\ v' & -E_d+2E_f-2U_{fc}+U_{ff}-E_L \end{bmatrix} . \tag{7}$$

U_{fc} is the attractive potential between the $3d$ core hole and a $4f$ electron, and E_d is the energy of the $3d$ level. According to Gunnarsson and Jepsen,[15] hybridization may strongly depend upon the electron configuration. So we denote the effective hybridization in the final state by $v'=\sqrt{13}V'$. We first assume that all other parameters are common for the $4f$ and $3d$ photoemission. By diagonalizing this matrix, the final states are represented as

$$\Psi_{d\pm}=c_{1\pm}^d|3d^94f^1\rangle+c_{2\pm}^d|3d^94f^2\underline{L}\rangle \tag{8}$$

and their energies $E_\pm$ are obtained. The intensities of the peaks are represented as

$$I_{d\pm}=|c_1^{i*}c_{1\pm}^{d}+c_2^{i*}c_{2\pm}^{d}|^2 . \quad (9)$$

Deconvolution of the $3d_{3/2}$ peak yields $E_+-E_-=4.8$ eV and $I_{d-}/I_{d+}=0.18$. Using these values, we can evaluate the difference of the diagonal elements of Eq. (7) $E_f-U_{fc}+U_{ff}-E_L$ and the hybridization V', only if the initial state Ψ_i [see Eq. (3)] is known. It is noted that Ψ_i is determined by E_f, E_L, U_{ff}, and V [see Eq. (1)], and E_f, E_L, and U_{ff} are obtained as functions of V [Fig. 5(a)] from the present analysis of the $4f$ photoemission. In this way, Ψ_i is given as a function of V. Therefore, V' and U_{fc} (instead of $E_f-U_{fc}+U_{ff}-E_L$ since E_f,U_{ff}, and E_L are functions of V) can be obtained as functions of V as shown in Fig. 5(b).

Using $V=0.22(3)$ obtained above from $U_{ff}=6.4$, we get $V'=0.34$ and $U_{fc}=9.9$ (all values in eV) from Fig. 5(b). We note that the transfer integral is much larger in the $3d$ core photoemission final state than in the $4f$ photoemission final state. This situation that $V'>V$ does not significantly change as long as $V>0.215$ eV corresponding to $U_{ff}>5$ eV [see Fig. 5(a)], which seems to be a reasonable range of U_{ff}. This configuration dependence of the transfer integral seems to contradict the estimate by Gunarsson and Jepsen.[15] According to their *ab initio* calculation, V'^2 must be smaller than V^2 by nearly a factor of 2 for a Ce state whose ground state is $4f^1$.

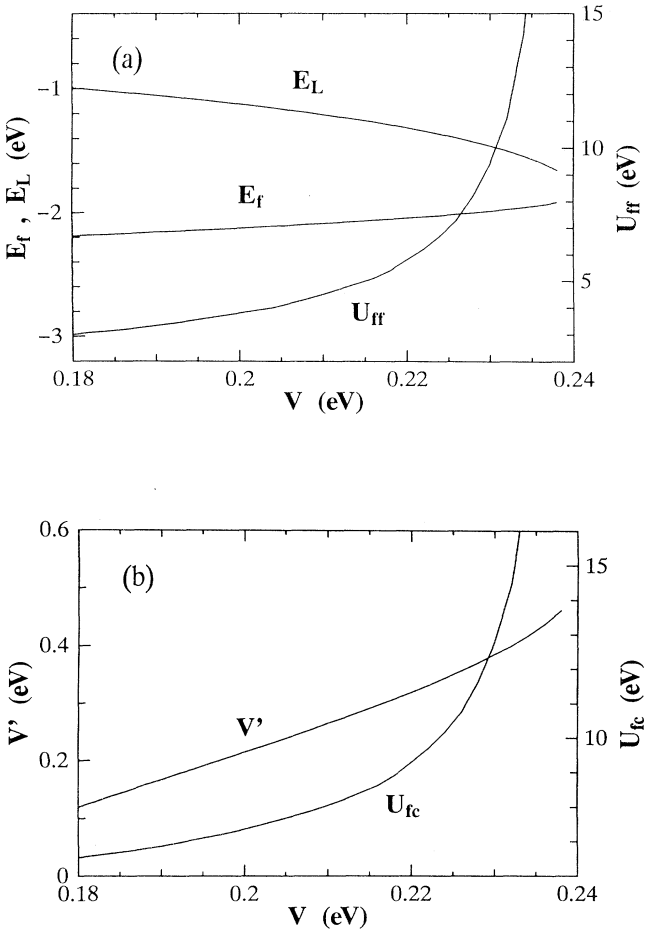

FIG. 5. Results of analysis of the photoemission spectra of CeB_6. (a) Deconvoluted spectrum of Fig. 3, spectrum C is used for the analysis. Choosing V as an independent variable, U_{ff}, E_f, and E_L are obtained as functions of V. (b) Deconvolution of the $3d_{3/2}$ signal is used for the analysis. U_{fc} and V' are obtained as functions of V using U_{ff}, E_f, and E_L shown in (a) as functions of V.

In order to account for this peculiar behavior of the transfer integral, we have to examine the employed model. The present ligand level represents the portion of the ligand band which most strongly hybridizes with the $4f$ state. This portion may depend upon the individual configuration as explained later. It is also recognized that the hybridization between the $4f$ state and the portion of the ligand band may depend upon the density of states and the character of the state. The above result that $V'>V$ strongly suggests that the relevant part of the ligand band is different between the final state of the $3d$ and $4f$ photoemission.

For an advanced analysis on the basis of this concept, at least three ligand levels should be considered, namely, one representing the relevant part of the ligand band in the initial state L_i, one in the $4f$ photoemission final state L_f, and one in the $3d$ photoemission final state L_d. For a consistent analysis, we have to take into account four bases in every configuration. In the initial state, for example, four bases, $|f^1\rangle$, $|f^2\underline{L}_i\rangle$, $|f^2\underline{L}_f\rangle$, and $|f^2\underline{L}_d\rangle$, should be considered. Then, the dimension of the matrices to be dealt with would become four instead of two in the above analysis. Also, a deconvolution of the spectra into four components is required. This process will yield much more ambiguity than the deconvolutions into two components. Hence, thus obtained parameters will not have quantitative reliability.

Consequently we here apply the simplest model in order to qualitatively clarify the mechanism for providing $V'>V$ in the present photoemission spectra. In this model the initial state is assumed to be a pure f^1 state and the ligand band at E_{Li} is ignored. In the final state of the $4f$ ($3d$) photoemission, we consider only the L_f (L_d) ligand band with energy E_{Lf} (E_{Ld}), and denote the hybridization between this state with the $4f$ level by V_f (V_d). Then, we get (in eV) $E_f=-1.9$, $E_{Lf}=-1.7$, and $V_f=0.24$ from the $4f$ photoemission, and $E_f-U_{fc}+U_{ff}-E_{Ld}=-3.3$ and $V_d=0.47$ from the $3d$ photoemission. The quantitative difference between the present V_d and V' obtained above is not of any significance, since the larger V_d results from the omission of the f^2 contribution in the initial state.

According to the band-structure calculation,[3] the main part of the valence band is located between $E_B=3.5$ and 6.5 eV. In the case of the $4f$ resonance photoemission, the density of state is quite small at the portion of the band around $E_B=-E_{Lf}=1.7$ eV, which is found to be most strongly hybridized with the f state. This inevitably leads to a small value of V_f. The reason this part hybridizes strongly in spite of the small hybridization V_f is that it is near the $4f$ level.

In the case of the $3d$ XPS, let us define the "$4f$ level"

by $E_f' = E_f + U_{ff} - U_{fc}$. This is the energy that a ligand electron would take when it transfers to the $4f$ level. Our analysis has shown that $E_f' - E_{Ld} = -3.3$ eV. But $-E_{Ld}$ cannot be determined unless $E_f + U_{ff} - U_{fc}$ is known. According to Fuggle *et al.*,[14] $U_{ff} - U_{fc}$ may vary from about -3 eV to about -6.5 eV. Hence, the possible position of the $f^{n+1}(f^2)$ level is $4.9 < -E_f' < 8.4$ eV by considering $-E_f = 1.9$ eV, leading to $1.6 < -E_{Ld} < 5.1$ eV. If $-E_{Ld}$ is larger than 3.5 eV, this ligand level corresponds to the topmost part of the main valence band and the density of states will be appreciable. Then the value V_d can be much larger than V_f as found in the present case. There is one question why the ligand states around $-E_{Ld} \sim 4$ eV do not contribute much to the $4f$ resonance photoemission. This is because their energy ($-E_{Ld} \sim 4$ eV) is much different from the energy of the $4f$ level ($-E_f = 1.9$ eV) compared with $-E_{Lf} = 1.7$ eV.

V. CONCLUSION

R $3d$ x-ray absorption spectroscopy (XAS) spectra of CeB_6 and PrB_6 have shown structures reflecting the Ce^{3+} and Pr^{3+} character. The valence-band photoemission spectra of CeB_6 and PrB_6 have shown prominent resonance structures for the excitation in the *R* $3d \rightarrow 4f$ absorption region, which are attributed to the $4f$ states. For CeB_6, we have clearly observed a two-peak structure which corresponds to the bonding and antibonding combinations of the f^{n-1} and $f^n\underline{L}$ final state ($n = 1$). The spectrum of PrB_6 also suggests two components due to similar combinations ($n = 2$). Analyses of the spectra using a cluster model have yielded parameters such as V, $-E_f$, and $-E_L$, where V stands for the hybridization of the $4f$ state with the ligand band state. It is found that the effective hybridization V_f under the $4f$ photoemission excitation is much smaller than that under the $3d$ photoemission excitation V_d in CeB_6. The difference of the effective hybridizations V_f and V_d is induced because different parts of the ligand band preferentially hybridize with the $4f$ state in the final states of the two spectroscopies. Although the analysis based on a cluster model with replacing the ligand band with a single level is quite effective, it requires detailed knowledge about the band structure. In order to fully analyze the result, dependence of the transfer integral upon the position in the ligand band and also its configuration dependence should be calculated realistically, e.g., using the results of band-structure calculations.

ACKNOWLEDGMENTS

We wish to thank Professor A. Yagishita of the Photon Factory for facilitating the measurement of the resonance photoemission of CeB_6 and PrB_6. We also thank N. Shino, A. Kimuara, and T. Fukawa of Osaka University for their support during the experiments. This work was supported by Grant in Aid for Scientific Research from the Ministry of Education, Science and Culture, Japan and by Asahi Glass Science Foundation.

[1]K. Samwer and K. Winger, Z. Phys. B **25**, 269 (1976).

[2]T. Kasuya, K. Takegahara, Y. Aoki, K. Hanzawa, M. Kasaya, S. Kunii, T. Fujita, N. Sato, H. Kimura, T. Komatsubara, T. Furuno, and J. Rossat-Mignod, in *Valence Fluctuations in Solids,* edited by L. M. Falicov, W. Hanke, and M. B. Maple (North-Holland, Amsterdam, 1981), p. 215; Phys. Rev. B **21**, 1335 (1980).

[3]A. Hasegawa and A. Yanase, J. Phys. F **7**, 1245 (1977).

[4]H. Harima, O. Sakai, T. Kasuya, and A. Yanase, Solid State Commun. **66**, 603 (1988).

[5]T. Suzuki, T. Goto, T. Fujimura, T. Suzuki, and T. Kasuya, J. Magn. Magn. Mater. **52**, 261 (1985).

[6]B. I. Min and Y.-R. Jang, Phys. Rev. B **44**, 13 270 (1991).

[7]M. Campagna, G. K. Wertheim, and Y. Baier, in *Photoemission in Solids II,* edited by L. Ley and M. Cardona (Springer-Verlag, Berlin, 1979), p. 217.

[8]Y. Mori, N. Shino, S. Imada, S. Suga, T. Nanba, M. Tomikawa, and S. Kunii, Physica B **186-188**, 66 (1993).

[9]B. T. Thole, G. van der Laan, J. C. Fuggle, G. A. Sawatzky, R. C. Karnatak, and J.-M. Esteva, Phys. Rev. B **32**, 5107 (1985).

[10]M. Campagna and F. U. Hillebrecht, in *Handbook on the Physics and Chemistry of Rare Earths Vol. 10,* edited by K. A. Gschneider, Jr., L. Eyring, and S. Hufer (North-Holland, Amsterdam, 1987), p. 75.

[11]A. Kotani and H. Ogasawara, J. Electron Spectrosc. Relat. Phenom. **60**, 257 (1992); H. Ogasawara, A. Kotani, and B. T. Thole, ISSP Tech. Rep. A **2802**, 1 (1994).

[12]S. Kimura, H. Harima, T. Nanba, S. Kunii, and T. Kasuya, J. Phys. Soc. Jpn. **60**, 745 (1991).

[13]A. Fujimori, Phys. Rev. B **27**, 3992 (1983).

[14]J. C. Fuggle, F. U. Hillebrecht, Z. Zolnierek, R. Lasser, Ch. Freiburg, O. Gunnarsson, and K. Schonhammer, Phys. Rev. B **27**, 7330 (1983).

[15]O. Gunnarsson and O. Jepsen, Phys. Rev. B **38**, 3568 (1988).